RSC Advances

RSC Publishing

PAPER

View Article Online
View Journal | View Issue

Graphene supported α-MnO_2 nanotubes as a cathode catalyst for improved power generation and wastewater treatment in single-chambered microbial fuel cells†

Cite this: *RSC Advances*, 2013, **3**, 7902

Santimoy Khilari,[a] Soumya Pandit,[b] M. M. Ghangrekar,[c] Debabrata Das[b] and Debabrata Pradhan*[a]

Received 18th October 2012,
Accepted 12th March 2013

DOI: 10.1039/c3ra22569k

www.rsc.org/advances

Microbial fuel cells (MFC) are a promising system to simultaneously accomplish the goal of energy production and wastewater treatment. In the MFC, the cathode plays an important role in achieving high power density and thereby improving the cell performance. In the cathode, an allotrope of carbon [activated carbon, graphite, multi-walled carbon nanotubes (MWCNTs)] is commonly used as a support material for catalysts, such as Pt. Here we show the improved performance of single-chambered MFC (sMFC) using hydrothermally synthesized α-manganese dioxide nanotubes (MnO_2-NTs) as the catalyst and graphene as the support in the cathode. With a fixed MnO_2-NTs loading, a maximum volumetric power density of 4.68 W m^{-3} was achieved from the sMFC with MnO_2-NTs/graphene, which is higher than that of MnO_2-NTs/MWCNTs (3.94 W m^{-3}) and MnO_2-NTs/Vulcan XC (2.2 W m^{-3}) composite cathodes, but marginally lower than that of the benchmark Pt/C cathode (5.67 W m^{-3}). The MnO_2-NTs/graphene composite also showed a higher oxygen reduction reaction (ORR) activity than the MnO_2-NTs/MWCNTs and MnO_2-NTs/Vulcan XC composites implying that the former is a better catalyst than the later two. This study demonstrates the high ORR activity and high power generation ability of the cost-effective MnO_2-NTs/graphene composite and makes it a potential cathode material for the replacement of expensive Pt in constructing large-scale MFC for wastewater treatment and bioelectricity production.

1. Introduction

In recent years, microbial fuel cells (MFC) have been emerging as one of the promising alternate technologies for harvesting renewable energy through wastewater treatment in the form of electricity,[1–4] biohydrogen production,[5,6] and as a biological oxygen demand sensor.[7] However, to establish commercially successful MFC technology and to compete with the existing technology such as anaerobic digesters for wastewater treatment, it is necessary to reduce the cost of device fabrication along with the increment in power output.[8] The power generation in MFC is largely dependent on the reduction kinetics at the cathode. Hence, the electron acceptor in the cathode plays a vital role in the power generation of the MFC.[9] Instead of unsustainable high redox potential oxidants (ferricyanide, permanganate, persulfate and dichromate)[10] and low power generating nitrate and nitrites,[11] oxygen can be an effective electron acceptor in MFC for its high positive redox potential, natural abundance, and sustainability.[9] However, the sluggish nature of the oxygen reduction reaction (ORR) with catalyst-free graphite/carbon electrodes leads to a high reduction overpotential, which is among the most limiting factors in the performance of MFC.[9] Therefore, the introduction of new sustainable high efficiency catalysts for the ORR has become necessary for improved MFC performance.[12] Nobel metals such as platinum (Pt), gold (Au), palladium (Pd) and their alloys show promising catalytic properties towards ORR enhancement.[13–15] Among these, Pt-based catalysts are extensively used in fuel cell technology. However, the high cost and lack of potential stability, along with the catalyst poisoning, limit its application for large scale commercial use.[16] Substantial efforts have been made to improve the ORR kinetics at the cathode surface using

[a]*Materials Science Centre, Indian Institute of Technology, Kharagpur-721302, India. E-mail: deb@matsc.iitkgp.etnet.in*
[b]*Department of Biotechnology, Indian Institute of Technology, Kharagpur-721302, India*
[c]*Department of Civil Engineering, Indian Institute of Technology, Kharagpur-721302, India*

† Electronic supplementary information (ESI) available: The membrane cathode assembly, MFC test and operation, analytical measurement and calculation. Schematic of sMFC, FE-SEM images of MnO_2-NTs and composite cathodes, polarization plots for MnO_2 NTs-Vulcan XC composite cathode, plot of current density *vs.* external resistance for the sMFC with different composite cathodes. XRD patterns of α-MnO_2-NTs before and after electrochemical cycles. TEM image of α-MnO_2-NTs after electrochemical cycles. See DOI: 10.1039/c3ra22569k

inexpensive electro-catalysts such as transition metals, metal oxides, macrocycles (phthalocyanine and porphyrines), conducting polymers and carbon nanotubes (CNTs) supported nanostructures with limited success.[16–20]

Manganese oxides (MnO_x) have attracted much attention as cathode catalysts in MFC because of their abundance, low cost, environmental friendliness, and considerable catalytic activity towards the electrochemical ORR.[21] A few studies on MnO_x cathodes for MFC have been reported. Clauwaert *et al.* used electrochemically precipitated MnO_2 to treat graphite felt cathodes and compared the performance with a non-treated cathode.[22] After the start up, the cell performance was reported to be similar for both the cathodes. This might be due to large MnO_2 particles electrochemically produced and/or the use of a graphite fibers substrate which tends not to produce well-adhered electrodeposits.[22] Zhang *et al.* reported MnO_2 as an alternative cathode catalyst to Pt in the MFC.[23] A recent report showed that MnO_2-based air cathodes give better performance in fuel cells due to their ability to absorb or deliver a large quantity of charge in a short duration (flywhell effect).[24] Early reports have shown that the catalytic performance of MnO_x follows the sequence of $Mn_5O_8 < Mn_3O_4 < Mn_2O_3 <$ MnOOH and that among MnO_2 phases, the performance sequence is β- < λ- < γ- < α-MnO_2.[25–27]

The drawback of MnO_2 lies in its poor electrical conductivity which limits its electrochemical activity. Therefore, various types of conductive supporting materials (Vulcan XC-72, Monarch carbon black 1000, graphite) have been employed to enhance the electrochemical ORR performance. But these supporting materials have weak ORR activity.[28] So in order to improve the ORR performance of MnO_2, it can be incorporated to a better electron conducting material, such as MWCNTs or graphene, which possess outstanding electronic conductivity, chemical stability, better mechanical strength, high thermal stability, nano-size morphology and high activated surface area.[16,29,30] MnO_2 coated MWCNTs have been used as cathode catalysts in MFC and reported to show a better MFC performance.[16] However, the synthesis of MWCNTs is normally carried out at a higher temperature (>500 °C) in the presence of metal catalyst using the chemical vapour deposition technique and is therefore cost-ineffective to graphene. The presence of metal catalyst in the MWCNTs-based cathode can also have unwanted effects on the performance of MFC. In this prospect, graphene makes a good alternative to MWCNTs. Graphene consists of two dimensional single or few atomic layers of hexagonal carbon network that can be synthesized at room temperature using simple solution chemistry at a much lower cost than that of MWCNTs. Recently, graphene based materials have been found as potential materials for lithium ion batteries, supercapacitors, biosensors, photovoltaic cells, and catalysis for its very high surface area (theoretical value 2630 $m^2\ g^{-1}$), high conductivity, and easy synthesis process.[29–34] Nitrogen and sulphur doped graphene have been used as ORR catalysts in fuel cells.[35,36]

Considering the high catalytic performance of α-MnO_2[21] and superb electrical conducting property of graphene,[29,30] and MWCNTs, we report here the synthesis of α-MnO_2-NTs/graphene and α-MnO_2-NTs/MWCNTs composite cathode catalysts to be used in single-chambered MFCs (sMFC) as an air cathode. The performance of the MnO_2-NTs/graphene composite in terms of ORR activity, power generation, chemical oxygen demand (COD) removal and Coulombic efficiency (C_E) is compared with MnO_2-NTs/MWCNTs, MnO_2-NTs/Vulcan XC composites and benchmark Pt/C. The low manufacturing cost of the MnO_2-NTs/graphene composite and its high performance exhibits a great potential to replace Pt as a cathode catalyst for MFC applications in the large-scale wastewater treatment plants for efficient substrate removal and high power output.

2. Experimental details

2.1 Chemicals

Potassium permanganate ($KMnO_4$), hydrochloric acid (HCl) (35% v/v), potassium chloride (KCl), sodium nitrate ($NaNO_3$), hydrogen peroxide (H_2O_2), and all other chemicals were purchased from Merck (India) and used without further purification.

2.2 Synthesis of composite electrodes

MnO_2-NTs were synthesized using a simple and low temperature hydrothermal process. In a typical synthesis process, 10 mL of 1 M HCl was added to 30 mL of 0.06 M $KMnO_4$ solution and stirred for 15 min. The resulting mixture was transferred to a 50 mL Teflon-lined stainless steel autoclave and heated at 150 °C for 12 h in a muffle furnace. Then the furnace was allowed to cool down to room temperature naturally and the brown coloured precipitate formed inside the Teflon container was collected by centrifuge. The precipitate was first washed with distilled water several times and then with ethanol. Finally it was dried at 70 °C for 6 h.

The MnO_2-NTs/Vulcan XC composite was prepared by adding MnO_2-NTs and Vulcan XC-72 (purchased from Cabot corp., India) to a mixture of 20 mL acetone and 20 mL isopropanol. To the above mixture 0.5 mL of PTFE and 10 μL Nafion solution was added as a binder. The final solution was sonicated for 1 h and then sprayed on a preheated 36 cm^2 carbon paper (50 °C) (Alfa Aesar, India) using a gravity spray gun. The MnO_2-NTs/Vulcan XC composite on carbon paper was finally dried at 70 °C for 1 h for use as a cathode in the MFC. Three different MnO_2-NTs loadings (0.03, 0.1 and 0.3 mg cm^{-2}) were taken while keeping the final MnO_2-NTs and Vulcan XC quantity constant (0.35 mg cm^{-2}). The MnO_2-NTs/MWCNTs composite electrode was prepared in the same process as the MnO_2-NTs/Vulcan XC composite (0.3 mg cm^{-2} MnO_2-NTs loading) by replacing Vulcan XC with MWCNTs. MWCNTs were synthesized from the natural precursor camphor.[37]

Graphene was synthesized by reducing graphene oxide (GO) with sodium borohydride. GO was synthesized from graphite powder by a modified Hummer's method.[38] 100 mg of GO was dispersed in 250 mL distilled water by sonication for 2 h. The sonicated solution was then centrifuged to remove un-

exfoliated GO precipitated at the bottom of the container. Exfoliated GO solution was stirred overnight at room temperature. Then 100 mg $NaBH_4$ was added to the above solution and stirred for 30 min. The resulting $NaBH_4$ mixed solution was refluxed at 120 °C for 3 h in an oil bath with constant stirring. Black coloured graphene product was isolated by centrifuging and was dried at 70 °C for 12 h. MnO_2-NTs/graphene composite (0.3 mg cm^{-2} MnO_2-NTs loading) was prepared in a similar process to that of the MnO_2-NTs/Vulcan XC composite.

2.3 Catalyst characterization

The surface morphology of the as-synthesized catalysts was analysed by field emission scanning electron microscopy (FE-SEM) with a Zeiss Supra 40 FE-SEM. Transmission electron microscopy (TEM) and selected area electron diffraction (SAED) measurements of the as-synthesized samples were performed with Tecnai FEI TEM operated at 200 kV accelerating voltage. The crystallographic phase and structures of the as-synthesized composite catalysts were characterized by X-ray powder diffraction (XRD) with a Rigaku Ultima III diffractometer using Cu-Kα_1 irradiation at a power of 40 kV × 40 mA. All the XRD patterns were recorded in the two theta range of 10° and 80°.

Electrochemical analysis of the as-synthesized MnO_2-NTs and composite catalysts was performed by cyclic voltammetry (CV) with a CH instrument electrochemical analyzer. A three-electrode system was employed for all measurements where pristine MnO_2-NTs or composite coated carbon paper, Pt wire and Ag/AgCl (KCl saturated; +197 mV) served as the working, counter and reference electrode, respectively. CV was recorded at a 100 mV scan rate from 0.9 to −0.9 V in 1 M KCl. KCl solution was saturated with oxygen by air bubbling for 30 min before the experiment. The electrochemical impedance spectroscopic (EIS) analysis was performed in 1 M KCl and the same electrode configuration in the frequency range of 2 MHz to 100 mHz with perturbation amplitude of 5 mV. The membrane cathode assembly fabrication and operation of sMFC are presented in the ESI.† Fig. S1 shows a schematic of the sMFC.

3. Results and discussion

3.1 Morphology and crystal structure of the catalysts

The surface morphology of the as-prepared samples was studied using FE-SEM. Fig. S2(a) in the ESI† shows the hollow urchin-like frame composed of MnO_2-NTs. The diameter of each spherical urchin-like structure was found in between 5 and 7 μm. A magnified FE-SEM image [ESI,† Fig. S2(b)] clearly reveals that these urchin-like structures were assembled from nanotubes with an average diameter of ~90 nm and length in the range of 2 to 4 μm. Fig. S2(c) and S2(d) of ESI† show the FE-SEM images of MnO_2-NTs/MWCNTs and MnO_2-NTs/graphene composites, respectively. MWCNTs and graphene appeared as coil-like and flake-like structures, respectively. The morphology of the as-synthesized composites suggests quite a uniform distribution of MWCNTs or graphene and MnO_2-NTs in the respective composite. The microstructure of the as-synthesized MnO_2-NTs, graphene, MnO_2-NTs/MWCNTs and MnO_2-NTs/graphene composite samples was analyzed by TEM. Fig. 1(a) shows a TEM image of MnO_2-NTs with outer diameters of 50–95 nm in accordance with the FE-SEM analysis. The corresponding high-resolution TEM (HR-TEM) image of the MnO_2-NTs [Fig. 1(b)] and the spot SAED pattern [inset, Fig. 1(b)] confirm the highly single crystalline nature of the MnO_2-NTs. An average *d*-spacing of about 0.47 nm was measured from the lattice resolved HR-TEM image, consistent with the spacing between (200) planes. Fig. 1(c) shows the TEM image of the as-synthesized graphene as a thin sheet-like microstructure with a few folded portions. The SAED from the graphene sheet shows ring pattern with dispersed bright spots, unlike the symmetric hexagonal lattice normally obtained for the single-layer graphene sheet.[39] The observed difference could be attributed to a few layers of graphene with disorientation in the folded regions and defects.[35,40] The TEM images of both MnO_2-NTs/MWCNTs (not shown) and MnO_2-NTs/graphene composites [Fig. 1(d)] reveal that the MnO_2-NTs were entangled with MWCNTs or graphene sheets.

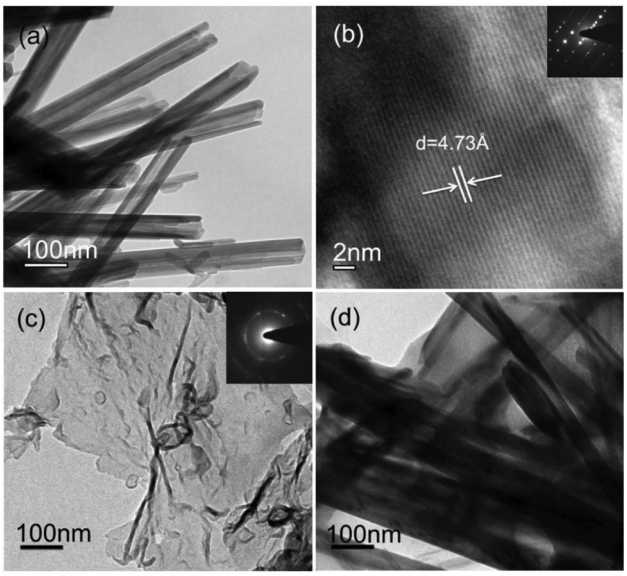

Fig. 1 TEM images of (a) hydrothermally synthesized MnO_2-NTs, (b) lattice from the wall of MnO_2-NTs, (c) graphene and (d) MnO_2-NTs/graphene composite. Insets of (b) and (c) show the SAED patterns.

Fig. 2 displays the XRD patterns of the as-synthesized MnO_2-NTs, graphene, MnO_2-NTs/Vulcan XC, MnO_2-NTs/MWCNTs and MnO_2-NTs/graphene composite samples. The XRD pattern [Fig. 2(a)] from pure MnO_2-NTs shows sharp diffraction features indicating the crystalline nature in agreement with the SAED pattern [inset, Fig. 1(b)]. The individual diffraction features from MnO_2-NTs were assigned and matched the α-MnO_2 phase with a tetragonal crystal system (JCPDS File No. 44-0141). The calculated lattice parameters of a = 9.781 Å and c = 2.857 Å also matched the reference value of a = 9.785 Å and c = 2.863 Å. The as-synthesized graphene shows a weak diffraction feature of (002) crystal plane at 2θ of 23.4° [Fig. 2(b)] with a larger *d*-spacing of 3.7 Å than that of

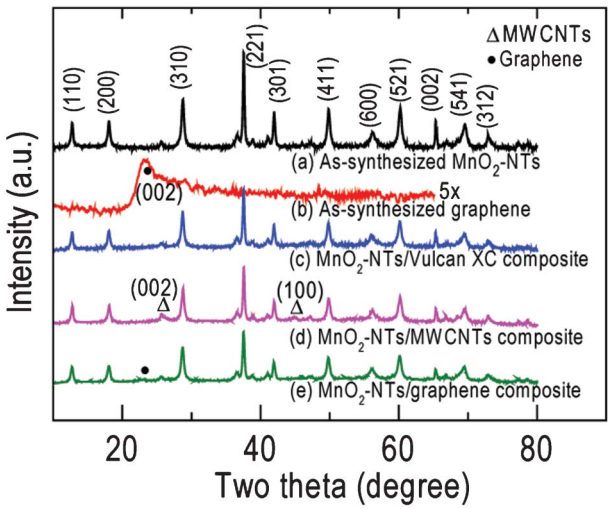

Fig. 2 XRD patterns of (a) MnO_2-NTs, (b) graphene, (c) MnO_2-NTs/Vulcan XC, (d) MnO_2-NTs/MWCNTs and (e) MnO_2-NTs/graphene composites.

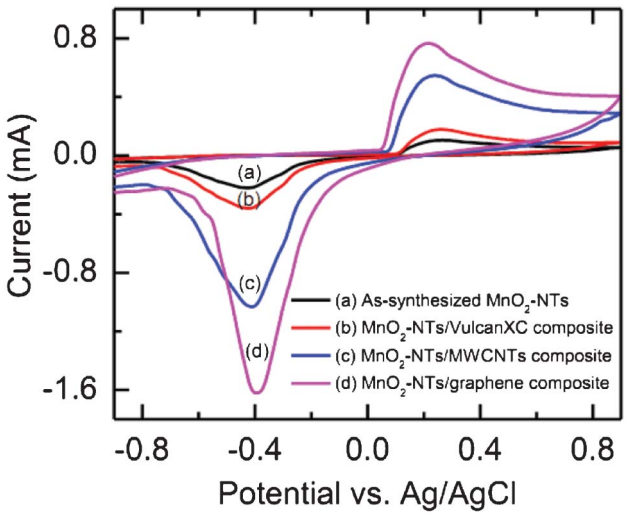

Fig. 3 Cyclic voltammograms of (a) the as-synthesized MnO_2-NTs, (b) MnO_2-NTs/Vulcan, (c) MnO_2-NTs/MWCNTs, and (d) MnO_2-NTs/graphene composites in air saturated 1 M KCl solution.

graphite, 3.4 Å. This increased *d*-spacing indicates the presence of oxygen containing groups and/or structural defects in the graphene.[29] This is in agreement with the ring SAED pattern obtained from the as-synthesized graphene [inset, Fig. 1(c)]. The XRD patterns of MnO_2-NTs/Vulcan XC, MnO_2-NTs/MWCNTs and MnO_2-NTs/graphene composite samples are shown in Fig. 2(c)–2(e), respectively. Due to the amorphous nature of Vulcan XC, only diffraction features from MnO_2-NTs are observed from the MnO_2-NTs/Vulcan XC composite. The MWCNTs show characteristic diffraction features at 2θ of 26° and 44.7° for (002) and (100) planes, respectively, in the MnO_2-NTs/MWCNTs composite [Fig. 2(d)]. The MnO_2-NTs/graphene composite shows diffraction features from both MnO_2-NTs and graphene [Fig. 2(e)].

3.2 Electrochemical ORR activity and the charge transport property of MnO_2-NTs and composite electrodes

The mechanism of the ORR can be investigated by various electrochemical methods including CV. Two distinct ORR mechanisms have been reported for the reduction of O_2 to OH^- and both the pathways compete with one another. These two mechanisms are (i) a four electron process to combine oxygen with electrons and protons directly (eqn (1)), when coupled with oxidation at the anode, to produce water as the end product and (ii) a less efficient, two step, two electron pathway involving the hydrogen peroxide ion (HO_2^-) as an intermediate (eqn (2)), followed by either two electron reduction of HO_2^- (eqn (3a)) or disproportionation in the reaction medium (eqn (3b)).[12] MnO_x favours the four electron ORR path and terminates the formation of corrosive peroxide.[25,27]

$$O_2 + 4H^+ + 4e^- \rightarrow 2H_2O \quad (1)$$

$$O_2 + 2H_2O + 2e^- \rightarrow HO_2^- + OH^- \quad (2)$$

$$HO_2^- + H_2O + 2e^- \rightarrow 3OH^- \quad (3a)$$

$$2HO_2^- \rightarrow 4OH^- + O_2 \quad (3b)$$

The electrochemical ORR activity of the as-synthesized MnO_2-NTs and composite catalyst coated carbon paper was studied by performing CV in air-saturated 1.0 M KCl solution. All the composite catalysts (MnO_2-NTs/Vulcan XC, MnO_2-NTs/MWCNTs and MnO_2-NTs/graphene) including the as-synthesized MnO_2-NTs showed a distinct oxygen reduction peak near −0.4 V, as shown in Fig. 3. This oxygen reduction peak is due to the insertion of a proton into MnO_2 as per the following (eqn (4)).[16]

$$MnO_2 + H_2O + e^- \rightarrow MnOOH + OH^- \quad (4)$$

The exact oxygen reduction peaks for the as-synthesized MnO_2-NTs, MnO_2-NTs/Vulcan XC, MnO_2-NTs/MWCNTs and MnO_2-NTs/graphene composites were found at −0.429 V, −0.425 V, −0.413 V and −0.397 V, respectively. The shift of the oxygen reduction peak towards a less negative potential is attributed to a decrease in the overpotential, which improves the ORR activity of the respective catalyst. In addition, the reduction peak currents for the MnO_2-NTs/graphene were found to be 1.57, 4.5 and 7.32 times higher than that of MnO_2-NTs/MWCNTs, MnO_2-NTs/Vulcan XC, and as-synthesized MnO_2-NTs, respectively. The observed higher current and low negative potential for the ORR is due to the large active surface area, low diffusion resistance to protons and easy electrolyte penetration through MnO_2-NTs/graphene, making it the best composite catalyst among these three composites prepared in the present work. Again the separation between the cathodic and anodic peaks was found to be the maximum for the as-synthesized MnO_2-NTs (0.69 V) and the minimum for MnO_2-NTs/graphene (0.613 V). This is an indication of a change in reversibility of the electrode materials. The minimum peak separation indicates less irreversibility of the MnO_2-NTs/

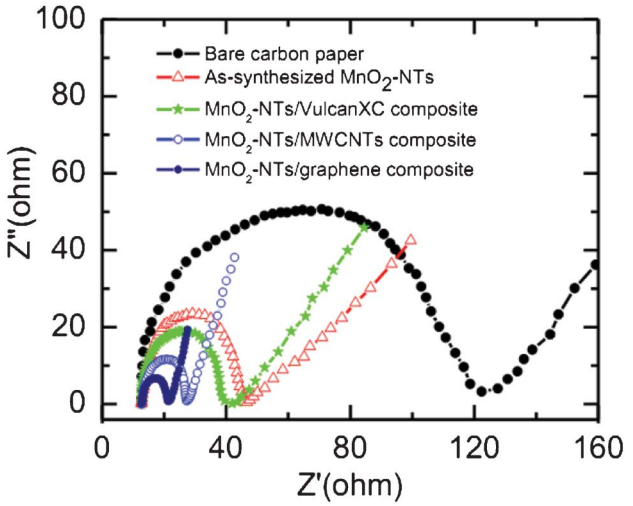

Fig. 4 Nyquist plots of the bare, as-synthesized MnO_2-NTs and composites coated carbon paper electrodes in 1 M KCl.

graphene composite, followed by the MnO_2-NTs/MWCNTs (0.652 V) and MnO_2-NTs/Vulcan XC (0.686 V) electrodes.

EIS analysis is extensively used to evaluate the charge transport behaviour of electroactive materials at the electrode/electrolyte interface. Generally Nyquist plots (imaginary component *vs.* real component of impedance) are utilized to study the interfacial electrochemical properties of the electrode. Fig. 4 shows the Nyquist plots of bare and different electrocatalysts coated carbon paper electrodes. All the plots have a well defined semicircle in the high frequency range, followed by a straight line in the lower frequency region. Charge transfer resistance (R_{ct}) of each electrode can be obtained from the diameter of the semicircles.[41] The R_{ct} value is directly related to the interfacial interaction between the catalyst and reactant or electrolyte. The measured R_{ct} value is found to follow the order of bare carbon paper (107.29 Ω) > as-synthesized MnO_2-NTs (33.03 Ω) > MnO_2-NTs/Vulcan XC (25.95 Ω) > MnO_2-NTs/MWCNTs (14.43 Ω) > MnO_2-NTs/graphene (8.61 Ω) electrode. A smaller R_{ct} value from the MnO_2-NTs/graphene electrode indicates the excellent charge transport. This faster electron transport increases the oxygen reduction rate in accordance to the highest reduction current obtained from the MnO_2-NTs/graphene composite (Fig. 3). A smaller R_{ct} is also responsible for the decrease in ORR overpotential for the MnO_2-NTs/graphene composite. The higher ORR activity and better charge transport property from the MnO_2-NTs/graphene composite is considered to be due to the two-dimensional platform structure of graphene, making it an excellent supporting matrix for MnO_2-NTs with much higher connectivity as compared to the spherical carbon particle (Vulcan) and one-dimensional MWCNTs. The graphene related compounds also have high adsorption abilities and are expected to be a good choice for adsorbent materials with the catalyst.[42] Furthermore, the excellent electronic conductivity of graphene, bestowed by its 2D planar π-conjugation structure,[43,44] can effectively transfer electrons to the MnO_2-NTs on which the electrochemical reduction of oxygen occurs, thereby improving the electrochemical performance.

3.3 Power generation from sMFC with a MnO_2-NTs loaded carbon composite cathode

Each batch cycle of the sMFC test was carried out for 36 h (±2 h). Initially the anaerobic anodic chamber of sMFC was fed with synthetic acetate wastewater without inoculation for 24 h. The pH of the wastewater was adjusted to 7.0 ± 0.1. An anodic half-cell potential of 192 ± 7 mV with respect to the Ag/AgCl reference electrode was recorded and no current was recorded during the absence of inoculum, implying the lack of biotic reaction in the anode chamber. Inoculation of the anodic chamber was carried out using an anaerobic consortia collected from the bottom sludge of the IIT Kharagpur septic tank. During the adaptation period (*i.e.* after inoculation), the sMFC was operated in a close circuitry configuration in fed-batch mode at ambient temperature (34 ± 2 °C). After inoculation, the anodic half-cell potential began decreasing owing to the donation of electrons to the anode by anodophiles and it reached at a plateau of about −289 ± 7 mV (*vs.* Ag/AgCl) against an external resistance of 100 Ω for all the MFCs. After 4 cycles, a stabilized performance of the anodic half cell was achieved.

With a stabilized anodic half-cell, the cathodic half-cell potential was measured with the different composite electrodes prepared in the present work. The effect of the MnO_2-NTs loading to carbon on the power generation in sMFC was studied by loading 0, 0.03, 0.1, 0.3 mg cm^{-2} MnO_2-NTs in Vulcan XC. A distinct difference in the cathodic half-cell potential was documented with different catalyst loading (MnO_2-NTs) in the air cathode of sMFC. The sMFC cathode with only Vulcan XC [without MnO_2-NTs *i.e.* catalyst-free] produced a maximum volumetric power density ($P_{d,max}$) of 0.57 W m^{-3}. Upon loading 0.03, 0.1 and 0.3 mg cm^{-2} MnO_2-NTs into Vulcan XC, the $P_{d,max}$ of the sMFC was increased to 0.93, 1.77 and 2.2 W m^{-3}, respectively (ESI,† Fig. S3 and Table S1). By increasing the MnO_2-NTs catalyst quantity in the Vulcan XC from 0 to 0.1 mg cm^{-2} a substantial enhancement (more than twice) of the $P_{d,max}$ is shown. However, increasing the MnO_2-NTs quantity from 0.1 to 0.3 mg cm^{-2} $P_{d,max}$ improved by only 24.29%. The maximum open circuit potential (OCP), C_E and COD removal efficiency were measured and found to be increased, whereas the internal resistance decreased with increasing the MnO_2-NTs loading into Vulcan XC (ESI,† Table S1). We conclude that the MnO_2-NTs content in the composite electrode significantly affects the power generation performance in the sMFC. The decrease in the internal resistance with MnO_2-NTs loading is attributed to the higher oxygen reduction kinetics at the cathode surface.

The sMFC performance of the MnO_2-NTs/Vulcan XC composite was then compared with the MnO_2-NTs/MWCNTs, MnO_2-NTs/graphene (with a fixed 0.3 mg cm^{-2} MnO_2-NTs loading) and benchmark Pt/C (with 0.3 mg cm^{-2} Pt loading) composites, and shown in Fig. 5. Polarization studies were performed after the sMFC reached a steady maximum in their OCP. The corresponding polarization curves of the sMFC, as shown in Fig. 5, were obtained by varying the external resistance from 30 Ω to 90 kΩ. It was observed that the

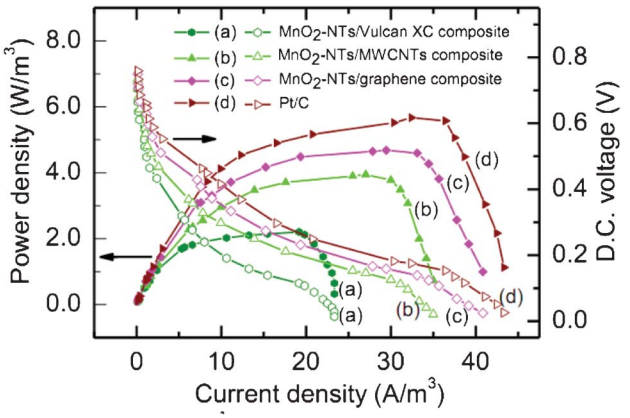

Fig. 5 Polarization plots for sMFC (power density and DC voltage as a function of current density) with different air cathodes (a) MnO_2-NTs/Vulcan XC (b) MnO_2-NTs/MWCNTs, (c) MnO_2-NTs/graphene, and (d) Pt/C composites. The power density and voltage data points are presented as solid and open symbols, respectively. A fixed quantity of catalyst (0.3 gm/cm^2 MnO_2-NTs or Pt) was loaded onto different carbon supports for comparison.

presence of MnO_2-NTs in the cathode induced a maximum OCP (754 mV) and higher $P_{d,max}$ ($\sim$2.2 W m^{-3}) than that of the catalyst-free cathode (only Vulcan XC) with OCP (677 mV) and $P_{d,max}$ ($\sim$0.57 W m^{-3}) as presented in Table 1. The power generation was found to decrease with an increase in external resistance indicating typical fuel cell behaviour. In addition, the potential drop was found to be very rapid at lower external resistance for sMFC with the catalyst-free cathode. When Vulcan XC was replaced with MWCNTs or graphene, an improvement in power generation was clearly observed as the $P_{d,max}$ of the former and latter were 3.94 W m^{-3} and 4.68 W m^{-3}, respectively. This may be attributed to the better electrical conductivity properties of the MWCNTs and graphene, as compared to Vulcan XC. To confirm this, an internal resistance was estimated using the current interruption method and it was measured to be 172, 108, 97, 85 and 75 Ω with catalyst-free, MnO_2-NTs/Vulcan XC, MnO_2-NTs/MWCNTs, MnO_2-NTs/graphene and Pt/C cathode catalyst, respectively. This decrease in the internal resistance is in agreement with the R_{ct} measured from the impedance spectra (Fig. 4). The sMFC with benchmark Pt/C cathode generated a $P_{d,max}$ of 5.67 W m^{-3} which is $\sim$21.15% higher than that of the MnO_2-NTs/graphene composite cathode. This result showed that the Pt/C cathode could be replaced with the MnO_2-NTs/graphene composite because of its high performance-to-cost ratio (discussed later). The larger surface area, better electronic conductivity and lower production-cost of graphene than that of MWCNTs make it a suitable candidate among different forms of carbon.[30] It is important to note that both the MnO_2-NTs/MWCNTs and MnO_2-NTs/graphene composite cathode show a significantly higher power generation ability than that of the electrochemically synthesized MnO_x cathode (0.772 W m^{-3}),[12] hydrothermally synthesized MnO_2 coated CNTs (2.54 W m^{-3}),[16] and hydrothermally synthesized MnO_2 (8.0 $\pm$ 0.2 mg cm^{-2} loading) with graphite as the conductive support (0.466 $\pm$ 0.019 W m^{-3}).[23] However, Wen *et al.* reported a 2.22 times higher $P_{d,max}$ (10.42 W m^{-3}) than that of the present work using birnessite-type MnO_2 nanoparticles loaded graphene.[41] This is due to a $\sim$14 times higher loading of MnO_2/graphene (5 mg cm^{-2}) in comparison to the present work *i.e.* 0.35 mg cm^{-2} of MnO_2-NTs/graphene loading. The lower $P_{d,max}$ (taking loading into consideration) obtained by Wen *et al.* can be attributed to the birnessite-type MnO_2 nanoparticles, which is known to show a poorer ORR activity than that of α-MnO_2.[45] The high $P_{d,max}$ obtained in the present work can therefore be attributed to the combined effect of the α-MnO_2 phase, NTs morphology, high crystallinity and superior electrochemical properties (ORR activity and excellent charge transport).

The power generation from sMFC is also influenced by the change in cathodic potential with respect to the OCP. In the case of the catalyst-free cathode, the more rapid decrease in cathodic potential from the OCP suggests poor reaction kinetics. The current density of cathodic half-cell is found to follow the following order: Pt/C benchmark > MnO_2-NTs/graphene > MnO_2-NTs/MWCNTs > MnO_2-NTs/Vulcan XC > catalyst-free electrode, at all the resistance values, indicating their order of catalytic performance (ESI,† Fig. S4). The observed comparable current density from the MnO_2-NTs/graphene with Pt/C could be attributed to the high ORR activity of MnO_2-NTs and the superior electrical properties of graphene.

The cathodic half-cell potential was also measured and found to increase with time in the cases of the Pt/C and MnO_2-NTs based electrodes, which is in contrast to several other cathodes where the cell potential decreases with time.[46,47] This signifies the importance of the MnO_2-based catalyst which behaves similarly to Pt/C. The increase in cathodic half-cell potential can be attributed to the increase in the pH of the catholyte in the presence of the cation exchange membrane (CEM). This is because of the migration of other cations (such as Na^+, K^+) instead of protons in the catholyte.[46,47] Recently, Cheng *et al.* and Qian *et al.* reported that MnO_2 shows improved ORR performance in an alkaline condition.[26,48] The

Table 1 Effect of the different carbon supports on the MnO_2-NTs based air cathode in the sMFC and a comparison with the benchmark Pt/C. A fixed quantity of catalyst (0.3 gm/cm^2 MnO_2-NTs or Pt) was loaded to the different carbon supports for comparison

sMFC with different cathode	Catalyst-free	MnO_2-NTs/Vulcan XC	MnO_2-NTs/MWCNTs	MnO_2-NTs/graphene	Benchmark Pt/C
Maximum OCP (mV)	677	754	793	812	839
Max.volumetric Power density (W m^{-3})	0.57	2.2	3.94	4.68	5.67
Max. coulombic efficiency (%)	5.0	8.4	11.0	11.5	12.6
COD removal efficiency (%)	69.23	78.7	82.9	83.7	84.37
Internal resistance (Ω)	172	108	97	85	75

pH imbalance is an obvious phenomenon in the case of MFC, since most cation species were transported from the anode to the cathode due to the concentration gradient. Another possible reason of pH increase could be due to the production of OH^- by water electrolysis (eqn (5)–(8)) at the cathode surface during ORR, particularly in non-buffered environments in the systems with membranes.[49] Although alkalinity adversely affects the performance of several cathodes in a non-buffered environment,[49] the opposite trend in the present work is attributed to the role of MnO_2-NTs, which in turn facilitates the ORR.[25,26] Several research groups have reported that MnO_2 shows an excellent catalytic property towards oxygen reduction in an alkaline medium. Cao *et al.* reported that the reduction of oxygen on an MnO_2 electrode in alkaline medium undergoes an efficient four electron pathway rather than a two electron pathway.[25] The ORR is achieved by the oxidation of Mn(III) species, generated from the auto-discharge of MnO_2 and the steps can be represented as the following[25]

$$Mn^{IV}O_2 + H_2O + e^- \rightleftharpoons Mn^{III}OOH + OH^- \quad (5)$$

$$2Mn^{III}OOH + O_2 \rightleftharpoons 2\left(Mn^{IV}OOH.O^-\right) \quad (6)$$

$$\left(Mn^{IV}OOH.O^-\right) + e^- \rightarrow Mn^{IV}O_2 + OH^- \quad (7)$$

A combination of eqn (5), (6) and (7) gives the four electron reduction of molecular oxygen as

$$O_2 + 2H_2O + 4e^- \rightarrow 4\ OH^- \quad (8)$$

The electroreduction of MnO_2 (Mn^{4+}) to MnOOH (Mn^{3+}) (eqn (5)) (not Mn^{2+}) can be explained by the presence of a reduction peak at ~ -0.4 V in the cathodic sweep (Fig. 3).[16] This is further confirmed by the presence of an anodic peak at ~ 0.2 V responsible for the oxidation of MnOOH to MnO_2 (Fig. 3).[50] In the case of the two electrons ORR path, H_2O_2 is an intermediate product.[25] In order to check the formation of H_2O_2, we have taken a UV-vis absorption spectrum of electrolyte collected after 20 cathodic sweeps. The collected electrolyte did not show any peak at 325 nm for H_2O_2 in the UV-vis spectrum (not shown) thereby confirming four electrons ORR pathways and H_2O_2 is not the major product. Further study is needed to ascertain if H_2O_2 formation occurs at a very low-level.[51,52] We have also collected the XRD measurement of α-MnO_2-NTs after 20 electrochemical cycles to observe any phase changes. The XRD pattern (ESI,† Fig. S5) was found to remain matched to the α-MnO_2 indicating no change in its phase after electrochemical cycles. The reduction in the XRD peak intensity after electrochemical cycles was due to a very small quantity of the MnO_2-NTs sample, which was collected by mechanically scratching the MnO_2-NTs coated carbon paper. The full-width-half-maximum of the most intense (221) XRD peaks were measured to be 0.247° and 0.25° for MnO_2-NTs catalyst before and after electrochemical cycles, suggesting negligible change in the crystalline property. The TEM image and spot SAED pattern (ESI,† Fig. S6) further confirm no change in the microstructural and structural properties of the MnO_2-NTs catalyst after 20 electrochemical cycles indicating its stability.

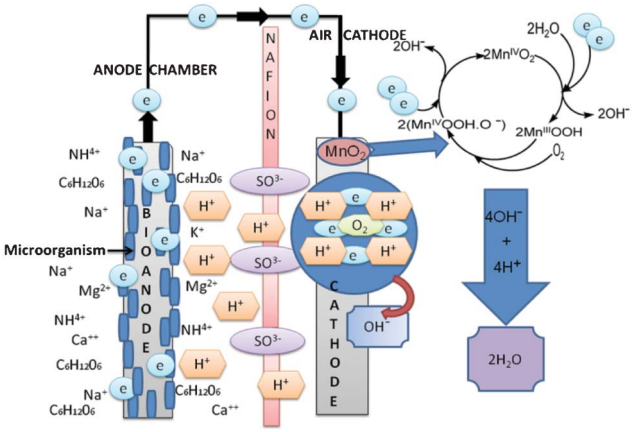

Fig. 6 A schematic of the sMFC displaying the process occurring at the anode and cathode during the power generation. The anode and cathode electrode were carbon cloth and MnO_2-NTs were supported on the different forms of carbon, respectively. Nafion 117 was used as the cation exchange member in the current sMFC test.

Fig. 6 shows a schematic of the process occurring in the sMFC with the MnO_2-NTs based cathode. The electrons are generated at the anode due to the biodegradation of organic waste (such as acetate) by exoelectrogen flow through the external circuit to MnO_2-NTs based cathode, where it electrochemically reduces O_2 into OH^- in the process producing electricity.

Fig. 7 shows the C_E (%) as a function of batch cycle with different air cathodes in the sMFC. The performance of all the air cathodes in the sMFC was found to be improved with the duration of operation and became stable after about 4 to 5 cycles of operation. The C_E (%) of the Vulcan XC cathode

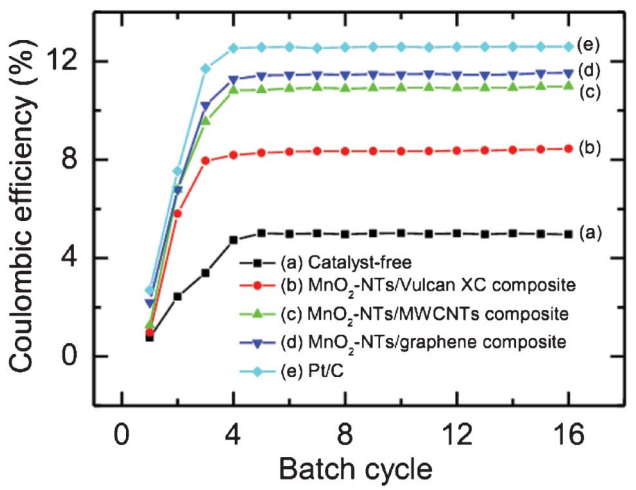

Fig. 7 Coulombic efficiency (%) of sMFC as a function of batch cycle with (a) catalyst-free, (b) MnO_2-NTs/Vulcan XC, (c) MnO_2-NTs/MWCNTs, (d) MnO_2-NTs/graphene, and (e) Pt/C composite cathodes. Each batch cycle was 36 h (±2 h).

(catalyst-free or MnO_2-NTs-free) was estimated to be about 5.0%, and it significantly increased to about 8.72% for the MnO_2-NTs/Vulcan XC composite suggesting the superior catalytic behaviour of the MnO_2-NTs for the sMFC. The C_E is further increased to ~11.0%, ~11.5% and ~12.6% for MnO_2-NTs/MWCNTs, MnO_2-NTs/graphene and Pt/C composite cathodes, respectively.

3.4 Wastewater treatment

MFC is documented as an effective wastewater treatment with simultaneous power generation.[3] The efficiency of sMFC suggests the COD removal from wastewater treatment. High COD removal (utilizing substrate/waste) enumerates the effective function of mixed microflora in the wastewater treatment. The COD removal in sMFC increased with MnO_2-NTs loading in Vulcan XC and showed the highest stable COD removal of 78.70% with 0.3 mg cm^{-2} MnO_2-NTs (ESI,† Table 1). MnO_2-NTs/MWCNTs and MnO_2-NTs/graphene showed a further increase of COD removal ability to 82.9% and 83.7%, respectively, which are close to the COD removal ability 84.37% of the benchmark Pt/C catalyst (Table 1). As the C_E is directly related to the wastewater treatment, the highest C_E obtained from the sMFC with MnO_2-NTs/graphene composite cathode (~11.5%) was also close to the benchmark Pt/C cathode (~12.6%), suggesting that the MnO_2-NTs loaded composite plays an important role in cathodic reduction which in turn enhances the anodic oxidation kinetics.[10] Acetate utilization reaction using exoelectrogen is represented below (eqn (9)).

$$\underset{(A)}{CH_3COO^-} + \underset{(B)}{4H_2O} \xrightarrow{microbial.oxidation} \underset{(C)}{2HCO_3^-} + \underset{(D)}{9H^+} + \underset{(E)}{8e^-} \quad (9)$$

$$K_c = \frac{[C]^2[D]^9[E]^8}{[A][B]^4} \quad (10)$$

The higher consumption of electrons and protons in the sMFC is considered to be a reason for the improved COD removal during wastewater treatment and energy output through the bioelectrochemical system.

3.5 Cost estimation of cathode catalysts

General cost estimates were made for the MnO_2-NTs/graphene composite cathode based on the retail cost of the materials used to manufacture it. The cost of the commercially prepared cathode with Pt loading was simply the retail cost. While the maximum manufacturing cost (including electricity consumption) of pure MnO_2-NTs, graphene, and MnO_2-NTs/graphene composite (with ~70% MnO_2-NTs loading) per gram were $3.84, $2.38, and $3.51 respectively, the price of benchmark Pt/C (with 10% Pt loading) was $26 dollar per gram (SIGMA, USA). Therefore, the cost of the benchmark Pt/C cathode catalyst is about 50 times higher than that of the MnO_2-NTs/graphene composite with an equal loading of MnO_2-NTs. This suggests that the incorporation of MnO_2-NTs as a catalyst instead of expensive Pt in the cathode of sMFC has a high potential to realize MFC for commercial applications.

4. Conclusions

The present study demonstrates a simple hydrothermal synthesis of single crystalline α-MnO_2-NTs and its similar behaviour to Pt as a catalyst for ORR in the sMFC air cathode. With increasing the MnO_2-NTs loading into the carbon matrix (Vulcan XC), the performance of the sMFC is found to improve in terms of OCP, $P_{d,max}$, C_E, COD removal and low resistance. Among the different carbon supports, graphene was demonstrated to be the best with the MnO_2-NTs/graphene composite showing the highest sMFC performance matching the benchmark Pt/C. Furthermore, MnO_2-NTs based cathode catalysts increase the alkalinity of the sMFC cathode, similar to that of Pt/C. The low cost-to-performance ratio of the MnO_2-NTs/graphene composite in the sMFC exhibits a greater potential to replace Pt as a cathode catalyst for MFC applications in large-scale wastewater treatment plants for efficient substrate removal and high power output.

Acknowledgements

This work is supported by the Department of Science and Technology (INT/Korea/*P*-02), Bhabha Atomic Research Centre, Department of Biotechnology and Ministry of New and Renewable Energy Sources (MNRE). Authors thank Dr Mukul Kumar, Meijo University, Japan for MWCNTs.

Notes and References

1 Y. Qiao, S.-J. Bao and C. M. Li, Electrocatalysis in microbial fuel cells-from electrode material to direct electrochemistry, *Energy Environ. Sci.*, 2010, **3**, 544–553.
2 D. Pant, A. Singh, G. V. Bogaert, S. I. Olsen, P. S. Nigam, L. Diels and K. Vanbroekhoven, Bioelectrochemical systems (BES) for sustainable energy production and product recovery from organic waste and industrial waste waters, *RSC Adv.*, 2012, **2**, 1248–1263.
3 P. Aelterman, K. Rabaey, P. Clauwaert and W. Verstraete, Microbial Fuel Cells for Wastewater Treatment, *Water Sci. Technol.*, 2006, **54**, 9–15.
4 C. Feng, F. Li, H. Liu, X. Lang and S. Fan, A dual-chamber microbial fuel cell with conductive film-modified anode and cathode and its application for the neutral electro-Fenton process, *Electrochim. Acta*, 2010, **55**, 2048–2054.
5 B. E. Logan, D. Call, S. Cheng, H. V. M. Hamelers, T. H. J. A. Sleutels, A. W. Jeremiasse and R. A. Rozendal, Microbial Electrolysis Cells for High Yield Hydrogen Gas Production from Organic Matter, *Environ. Sci. Technol.*, 2008, **42**, 8630–8640.
6 H. Liu, H. Hu, J. Chignell and Y. Fan, Microbial Electrolysis: Novel Technology for Hydrogen Production from Biomass, *Biofuels*, 2010, **1**, 129–142.
7 M. Kim, S. M. Youn, S. H. Shin, J. G. Jang, S. H. Han, M. S. Hyun, G. M. Gadd and H. J. Kim, Practical field application of a novel BOD monitoring system, *J. Environ. Monit.*, 2003, **5**, 640–643.

8 B. H. Kim, I. S. Chang and G. M. Gadd, Challenges in Microbial Fuel Cell Development and Operation, *Appl. Microbiol. Biotechnol.*, 2007, **76**, 485–494.
9 H. Rismani-Yazdi, S. M. Carver, A. D. Christy and O. H. Tuovinen, Cathodic Limitations in Microbial Fuel Cells: An Overview, *J. Power Sources*, 2008, **180**, 683–694.
10 S. Pandit, A. Sengupta, S. Kale and D. Das, Performance of Electron Acceptors in Catholyte of a Two-chambered Microbial Fuel Cell Using Anion Exchange Membrane, *Bioresour. Technol.*, 2011, **102**, 2736–2744.
11 M. A. Rodrigo, P. Cañizares and J. Lobato, Effect of the Electron-acceptors on the Performance of a MFC, *Bioresour. Technol.*, 2010, **101**, 7014–7018.
12 X.-W. Liu, X.-F. Sun, Y.-X. Huang, G.-P. Sheng, K. Zhou, R. J. Zeng, F. Dong, S.-G. Wang, A.-W. Xu and Z.-H. Tong, Nano-structured Manganese Oxide as a Cathodic Catalyst for Enhanced Oxygen Reduction in a Microbial Fuel Cell Fed with a Synthetic Wastewater, *Water Res.*, 2010, **44**, 5298–5305.
13 M. K. Carpenter, T. E. Moylan, R. S. Kukreja, M. H. Atwan and M. M. Tessema, Solvothermal Synthesis of Platinum Alloy Nanoparticles for Oxygen Reduction Electrocatalysis, *J. Am. Chem. Soc.*, 2012, **134**, 8535–8542.
14 C. Koenigsmann, E. Sutter, R. R. Adzic and S. S. Wong, Size- and Composition-Dependent Enhancement of Electrocatalytic Oxygen Reduction Performance in Ultrathin Palladium-Gold (Pd1-xAux) Nanowires, *J. Phys. Chem. C*, 2012, **116**, 15297–15306.
15 C. Koenigsmann, E. Sutter, T. A. Chiesa, R. R. Adzic and S. S. Wong, Highly Enhanced Electrocatalytic Oxygen Reduction Performance Observed in Bimetallic Palladium-Based Nanowires Prepared under Ambient, Surfactantless Conditions, *Nano Lett.*, 2012, **12**, 2013–2020.
16 Y. Zhang, Y. Hu, S. Li, J. Sun and B. Hou, Manganese Dioxide-coated Carbon Nanotubes as an Improved Cathodic Catalyst for Oxygen Reduction in a Microbial Fuel Cell, *J. Power Sources*, 2011, **196**, 9284–9289.
17 R. Bashyam and P. Zelenay, A Class of Non-precious Metal Composite Catalysts for Fuel Cells, *Nature*, 2006, **443**, 63–66.
18 M. Zhou, M. Chi, J. Luo, H. He and T. Jin, An Overview of Electrode Materials in Microbial Fuel Cells, *J. Power Sources*, 2011, **196**, 4427–4435.
19 J. M. Morris, S. Jin, J. Wang, C. Zhu and M. A. Urynowicz, Lead Dioxide as an Alternative Catalyst to Platinum in Microbial Fuel Cells, *Electrochem. Commun.*, 2007, **9**, 1730–1734.
20 F. Zhao, F. Harnisch, U. Schroder, F. Scholz, P. Bogdanoff and I. Herrmann, Application of pyrolysed iron(II) phthalocyanine and CoTMPP based oxygen reduction catalysts as cathode materials in microbial fuel cells, *Electrochem. Commun.*, 2005, **7**, 1405–1410.
21 L. Mao, D. Zhang, T. Sotomura, K. Nakatsu, N. Koshiba and T. Ohsaka, Mechanistic Study of the Reduction of Oxygen in Air Electrode with Manganese Oxides as Electrocatalysts, *Electrochim. Acta*, 2003, **48**, 1015–1021.
22 P. Clauwaert, D. V. Ha, N. Boon, K. Verbeken, M. Verhaege, K. Rabaey and W. Verstraete, Open Air Biocathode Enables Effective Electricity Generation with Microbial Fuel Cells, *Environ. Sci. Technol.*, 2007, **41**, 7564–7569.
23 L. Zhang, C. Liu, L. Zhuang, W. Li, S. Zhou and J. Zhang, Manganese Dioxide as an Alternative Cathodic Catalyst to Platinum in Microbial Fuel Cells, *Biosens. Bioelectron.*, 2009, **24**, 2825–2829.
24 I. Roche, K. Katuri and K. Scott, A Microbial Fuel Cell Using Manganese Oxide Oxygen Reduction Catalysts, *J. Appl. Electrochem.*, 2010, **40**, 13–21.
25 Y. L. Cao, H. X. Yang, X. P. Ai and L. F. Xiao, The Mechanism of Oxygen Reduction on MnO2-catalyzed Air Cathode in Alkaline Solution, *J. Electroanal. Chem.*, 2003, **557**, 127–134.
26 F. Cheng, Y. Su, J. Liang, Z. Tao and J. Chen, MnO_2-Based Nanostructures as Catalysts for Electrochemical Oxygen Reduction in Alkaline Media, *Chem. Mater.*, 2009, **22**, 898–905.
27 F. H. B. Lima, M. L. Calegaro and E. A. Ticianelli, Investigations of the Catalytic Properties of Manganese Oxides for the Oxygen Reduction Reaction in Alkaline Media, *J. Electroanal. Chem.*, 2006, **590**, 152–160.
28 I. Roche, E. Chaînet, M. Chatenet and J. Vondrák, Carbon-Supported Manganese Oxide Nanoparticles as Electrocatalysts for the Oxygen Reduction Reaction (ORR) in Alkaline Medium: Physical Characterizations and ORR Mechanism, *J. Phys. Chem. C*, 2006, **111**, 1434–1443.
29 C. Wang, D. Li, C. O. Too and G. G. Wallace, Electrochemical Properties of Graphene Paper Electrodes Used in Lithium Batteries, *Chem. Mater.*, 2009, **21**, 2604–2606.
30 D. A. C. Brownson, D. K. Kampouris and C. E. Banks, An overview of graphene in energy production and storage applications, *J. Power Sources*, 2011, **196**, 4873–4885.
31 S. Bong, Y. R. Kim, I. Kim, S. Woo, S. Uhm, J. Lee and H. Kim, Graphene supported electrocatalysts for methanol oxidation, *Electrochem. Commun.*, 2010, **12**, 129–131.
32 M. Pumera, Graphene in biosensing, *Mater. Today*, 2011, **14**, 308–315.
33 G. Kalita, M. S. Kayastha, H. Uchida, K. Wakita and M. Umeno, Direct growth of nanographene films by surface wave plasma chemical vapor deposition and their application in photovoltaic devices, *RSC Adv.*, 2012, **2**, 3225–3230.
34 G. Kalita, S. Sharma, K. Wakita, M. Umeno, Y. Hayashi and M. Tanemurab, A photoinduced charge transfer composite of graphene oxide and ferrocene, *Phys. Chem. Chem. Phys.*, 2013, **15**, 1271–1274.
35 L. Qu, Y. Liu, J.-B. Baek and L. Dai, Nitrogen-Doped Graphene as Efficient Metal-Free Electrocatalyst for Oxygen Reduction in Fuel Cells, *ACS Nano*, 2010, **4**, 1321–1326.
36 Z. Yang, Z. Yao, G. Li, G. Fang, H. Nie, Z. Liu, X. Zhou, X. Chen and S. Huang, Sulfur-Doped Graphene as an Efficient Metal-free Cathode Catalyst for Oxygen Reduction, *ACS Nano*, 2011, **6**, 205–211.
37 M. Kumar and Y. Ando, A simple method of producing aligned carbon nanotubes from an unconventional precursor Camphor, *Chem. Phys. Lett.*, 2003, **374**, 521–526.
38 W. S. Hummers and R. E. Offeman, Preparation of Graphitic Oxide, *J. Am. Chem. Soc.*, 1958, **80**, 1339.
39 A. C. Ferrari, J. C. Meyer, V. Scardaci, C. Casiraghi, M. Lazzeri, F. Mauri, S. Piscanec, D. Jiang, K. S. Novoselov and S. Roth, Raman Spectrum of Graphene and Graphene Layers, *Phys. Rev. Lett.*, 2006, **97**, 1874011–4.

40 M. K. Singh, E. Titus, G. Goncalves, P. A. A. P. Marques, I. Bdikin, A. L. Kholkinb and J. J. A. Gracio, Atomic-scale observation of rotational misorientation in suspended few-layer graphene sheets, *Nanoscale*, 2010, **2**, 700–708.

41 Q. Wen, S. Wang, J. Yan, L. Cong, Z. Pan, Y. Ren and Z. Fan, MnO_2-graphene hybrid as an alternative cathodic catalyst to platinum in microbial fuel cells, *J. Power Sources*, 2012, **216**, 187–191.

42 X. Zhang, X. Quan, S. Chen and H. Yu, Constructing graphene/InNbO4 composite with excellent adsorptivity and charge separation performance for enhanced visible-light-driven photocatalytic ability, *Appl. Catal., B*, 2011, **105**, 237–242.

43 Q. J. Xiang and J. G. Yu, Graphene-based semiconductor photocatalysts, *Chem. Soc. Rev.*, 2012, **41**, 782–986.

44 X. An and J. C. Yu, Graphene-based photocatalytic composites, *RSC Adv.*, 2011, **1**, 1426–1434.

45 W. Xiao, D. Wang and X. W. Lou, Shape-Controlled Synthesis of MnO2 Nanostructures with Enhanced Electrocatalytic Activity for Oxygen Reduction, *J. Phys. Chem. C*, 2010, **114**, 1694–1700.

46 R. A. Rozendal, H. V. Hamelers and C. J. Buisman, Effects of Membrane Cation Transport on pH and Microbial Fuel Cell Performance, *Environ. Sci. Technol.*, 2006, **40**, 5206–5211.

47 S. Pandit, S. Ghosh, M. M. Ghangrekar and D. Das, Performance of an Anion Exchange Membrane in Association with Cathodic Parameters in a Dual Chamber Microbial Fuel Cell, *Int. J. Hydrogen Energy*, 2012, **37**, 9383–9392.

48 Y. Qian, S. Lu and F. Gao, Synthesis of Manganese Dioxide/reduced Graphene Oxide Composites with Excellent Electrocatalytic Activity Toward Reduction of Oxygen, *Mater. Lett.*, 2011, **65**, 56–58.

49 S.-J. You, N.-Q. Ren, Q.-L. Zhao, P. D. Kiely, J.-Y. Wang, F.-L. Yang, L. Fu and L. Peng, Improving Phosphate Buffer-free Cathode Performance of Microbial Fuel Cell Based on Biological Nitrification, *Biosens. Bioelectron.*, 2009, **24**, 3698–3701.

50 D. Soundararajan, Y. I. Kim, J.-H. Kim, K. H. Kim and J. M. Ko, Hydrothermal Synthesis and Electrochemical Characteristics of Crystalline α-MnO_2 Nanotubes, *Science of Adv. Mater.*, 2012, **4**, 805–812.

51 C.-H. Feng, F.-B. Li, H.-J. Mai and X.-Z. Li, Bio-Electro-Fenton Process Driven by Microbial Fuel Cell for Wastewater Treatment, *Environ. Sci. Technol.*, 2010, **44**, 1875–1880.

52 L. Liu, Y. Yuan, F.-B. Li and C.-H. Feng, In situ Cr(VI) reduction with electrogenerated hydrogen peroxide driven by iron-reducing bacteria, *Bioresour. Technol.*, 2011, **102**, 2468–2473.